THE JOURNAL OF PHYSICAL CHEMISTRY C
A JOURNAL OF THE AMERICAN CHEMICAL SOCIETY

pubs.acs.org/JPCC

Article

Efficient Routes for the Preparation of Urazole Radical Self-Assembled Monolayers on Gold Surfaces

Ángel Campos-Lendinez, Núria Crivillers,* Stefan T. Bromley, Concepció Rovira, Gary W. Breton,* and Marta Mas-Torrent*

Cite This: J. Phys. Chem. C 2022, 126, 13358−13365

Read Online

ACCESS | Metrics & More | Article Recommendations | Supporting Information

ABSTRACT: The functionalization of substrates with radical species has been shown to be a promising strategy to confer novel physical and chemical properties to a surface. Urazole radicals are persistent nitrogen-centered radicals that are insensitive to oxygen, making them desirable targets for the functionalization of surfaces. Here, we succeed in the preparation of self-assembled monolayers (SAMs) of a 1-arylurazole radical on Au surfaces using two different approaches. In the first approach, a SAM of a radical precursor on the gold surface is prepared followed by its chemical oxidation to generate the active urazole radical. In the second route, the radical is generated in solution and subsequently grafted on the Au surface. In both cases, the SAMs exhibit active radical behavior, but the SAM prepared by the first approach demonstrates greater surface coverage of the electroactive urazole radical species.

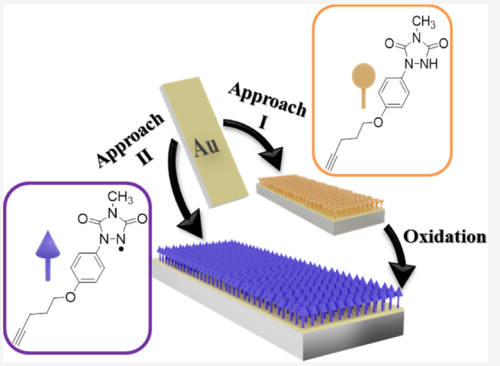

INTRODUCTION

The functionalization of substrates with organic molecules has proven to be a promising strategy to confer novel physical and chemical properties to surfaces. This route has been successfully exploited for the fabrication of chemical sensors,[1−3] for immobilizing biomolecules,[4−6] and for tuning surface wettability[7,8] or metal work function,[9] among other applications. In particular, surface modification with stable neutral organic radicals with one or more unpaired electrons has recently attracted great attention in the fields of molecular electronics and spintronics.[9−12]

Stable neutral organic radicals have been physisorbed on surface showing the Kondo effect.[13−15] However, to better stabilize such systems for potential applications, the preparation of self-assembled monolayers (SAMs) chemically bonded to the surface is often preferred.[16,17] This has been mainly realized by designing and synthesizing neutral organic radicals bearing appropriate surface anchors, for example, thiol or silane groups to graft the molecules onto Au or oxide substrates, respectively. In this way, SAMs of polychlorinated trityl radicals,[16,18] nitroxyls,[19,20] and α-nitronyl nitroxyls[21,22] have been widely investigated. Importantly, all of these radicals need to be highly stable to survive the reaction conditions required to prepare the SAMs and, further, the radical character needs to be preserved after the surface self-assembly process. To date, very few examples have been reported regarding the preparation of SAMs using precursors to radical species that are subsequently converted to their corresponding neutral radical analogues by performing surface chemical reactions[23] or by interaction with a metallic surface.[24]

Urazole radicals, **2**, which are readily accessible by oxidation of urazole precursors **1**, were first reported by Pirkle as early as 1978 (Scheme 1).[25] Many of these nitrogen-centered radicals are indefinitely persistent in solution.[25] While they are known to be in equilibrium with the corresponding N−N dimers **3** (Scheme 1), significant concentrations of the radical species remain present in the solution.[25−27] The unusual stability of these radicals, coupled with their lack of sensitivity to oxygen, make them desirable targets for the functionalization of surfaces. 1-Arylurazoles radicals are easily synthesized by established means and, therefore, in this paper have been selected as initial targets for studying the feasibility of SAM preparation.[25,26] Although 1-arylurazoles radicals such as **2b** are persistent in solution for many hours like other urazole radicals, they eventually succumb to a self-reaction to form urazole **4**.[25,26] Therefore, suitable methodologies have to be applied to successfully achieve radical urazole SAMs.

In this work, we report the preparation and characterization of urazole radical SAMs employing two different approaches. The first route is based on prior preparation of a SAM using the precursor to the radical species, followed by oxidization to the corresponding radical form. In the second approach, the radical is first generated in solution and then self-assembled on

Received: April 10, 2022
Revised: July 14, 2022
Published: July 27, 2022

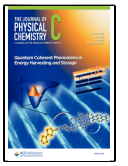

https://doi.org/10.1021/acs.jpcc.2c02453
J. Phys. Chem. C 2022, 126, 13358−13365

Scheme 1. Formation of Urazole Radicals 2 from Urazole Precursors 1[a,b]

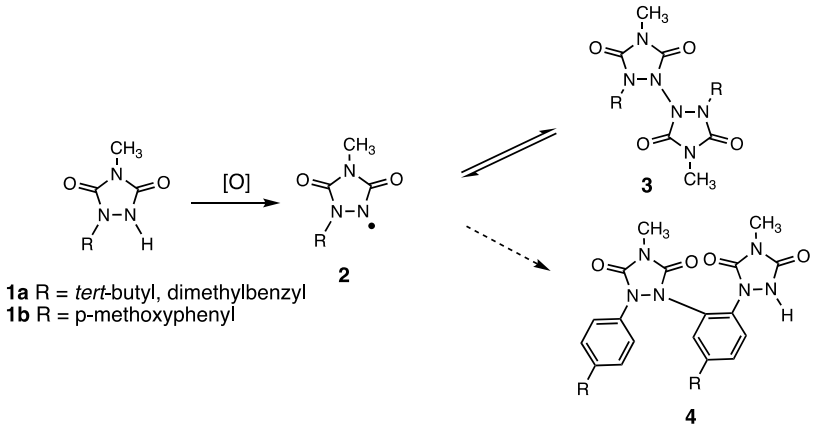

[a]The radicals are in equilibrium with N−N dimers **3** in solution. [b]Urazole radical **2b** undergoes a slow self-reaction to form **4**.

the surface. Both approaches successfully lead to urazole radical SAMs, as demonstrated by means of electrochemical and electron paramagnetic resonance (EPR) detection.

EXPERIMENTAL SECTION

General Methods for the Synthesis. Column chromatography was conducted on a silica gel (234−400 mesh). Thin-layer chromatography was performed on precoated silica gel plates and visualized by ultraviolet light. ^{1}H and ^{13}C NMR spectra were obtained on a 400 MHz NMR spectrometer. Chemical shifts are reported in units of parts per million downfield from TMS. High-resolution mass spectra (HRMS) were acquired via electron spray ionization on a Linear ion trap-Fourier transform hybrid mass spectrometer (LTQ-FTMS). *N*-methyl-1,3,5-triazoline-3,5-dione (**2**) was synthesized via oxidation of *N*-methylurazole with DABCO-Br_2 as described in the literature.[28,29] All other chemicals and solvents were obtained from commercial sources and used without further purification unless otherwise noted.

*(Pent-4-yn-1-yloxy)benzene (**5**).* To a solution of 1 g (10.6 mmol) of phenol in 25 mL of dry DMF, 1.19 g (1 equiv) of potassium *tert*-butoxide was added as a solid, at once, and stirred for 0.5 h. To the resulting pale green solution, 1.0 g (1 equiv) of 5-chloro-1-pentyne was added dropwise, and the reaction mixture was stirred overnight. The resulting pale brown mixture was poured into 50 mL of EtOAc, and the combined organic layer was washed with 2 × 50 mL of H_2O and 2 × 20 mL of sat. aq. NaCl, dried over Na_2SO_4, and concentrated. Column chromatography (SiO_2, 6:1 hexanes/EtOAc) afforded 1.12 g (60% yield) of **5** as a clear colorless liquid: ^{1}H NMR ($CDCl_3$) δ 7.26 (dt, J = 7.3, 8.5 Hz, 2H), 6.92 (t, J = 7.3 Hz, 1H), 6.89 (d, J = 8.5 Hz, 2H), 4.03 (t, J = 6.2 Hz, 2H), 2.38 (dt, J = 2.7, 6.9 Hz, 2H), 1.95−2.04 (m, 3H); ^{13}C NMR ($CDCl_3$) δ 158.9, 129.5, 120.8, 114.5, 83.6, 69.0, 66.0, 28.3, 15.3. HRMS [ESI] m/z [M + H]+ Calcd for $C_{11}H_{13}O$: 161.09609; Found 161.09616.

*4-Methyl-1-[4-(pent-4-yn-1-yloxy)phenyl]-1,2,4-triazolidine-3,5-dione (**6**).* To a stirring solution of 0.92 g (5.75 mmol) of compound **5** (neat) and 0.113 g (1 mmol) of MeTAD, 155 μL (2 mmol) of CF_3CO_2H was added via syringe. The solution initially turned deep red-purple in color, but then a thick white precipitate was formed. The precipitate was suspended in 10 mL of CH_2Cl_2 in a separatory funnel, and 2 mL of 1 M NaOH was added, which dissolved the precipitate. The aqueous layer was washed with 1 × 2 mL of CH_2Cl_2 and then acidified with conc. aq. HCl, forming a thick white precipitate. Washing with 3 × 50 mL of CH_2Cl_2, drying over Na_2SO_4, and concentration afforded 0.134 g (49% yield) of **6** as a white solid: ^{1}H NMR (DMSO-d_6) δ 11.05 (s, 1H, NH), 7.43 (d, J = 9.1 Hz, 2H), 7.01 (d, J = 9.1 Hz, 2H), 4.03 (t, J = 6.9 Hz, 2H), 2.96 (s, 3H), 2.83 (t, J = 2.6 Hz, 1H), 2.32 (dt, J = 2.6, 6.9 Hz, 2H), 1.88 (p, J = 6.9 Hz, 2H); ^{13}C NMR ($CDCl_3$) δ 156.4, 154.2, 151.6, 130.5, 121.3, 115.4, 84.2, 72.2, 66.7, 28.2, 25.4, 15.0. HRMS [ESI] m/z [M + H]+ Calcd for $C_{14}H_{16}N_3O_3$: 274.11862; Found 274.11824.

*Generation of a Urazole Radical (**7**).* To a stirring mixture of 3.35 mg of **6**, 13.65 mg of sodium sulfate (Na_2SO_4, 99.5%, Sigma) and 6.82 mg of nickel peroxide (Ni_2O_3 99%, Sigma) in 10 mL of acetonitrile was added. The solution, kept in inert conditions, turned blue after a few minutes. The mixture was stirred for 30 min and then filtered, resulting in a deep purple solution of radical **7**.

SAMs' Preparation and Characterization. SAMs were prepared on Au substrates (50 nm thick) evaporated on glass, purchased from Phasis Sàrl.

Approach I. The gold surface was cleaned in a piranha bath 1:1 (H_2SO_4/H_2O_2) for a minute and subsequently rinsed with plenty of Milli-Q water and ethanol, and dried with a N_2 stream. Afterward, the substrate was immersed in a 10^{-4} M solution of **6** in dry acetonitrile and was left for 48 h under stirring and inert conditions. Then, the substrates were rinsed with acetonitrile and ethanol to remove the physisorbed molecules, and dried with N_2, giving SAM **S6**. The resulting substrate was immersed in a previously prepared oxidant dispersion (6.82 mg of NiO_2 and 13.65 mg of Na_2SO_4 in 10 mL of acetonitrile heated at 50 °C for 30 min. in an ultrasound bath and in inert conditions) while stirring at low rpm. for 45 min. Afterward, the substrate was rinsed with plenty of acetonitrile, and ethanol and dried with a N_2 stream, affording SAM **S7-I**.

Approach II. The Au surface was cleaned as in approach I. Subsequently, the substrate was directly immersed into a 10^{-4} M solution of **7** in acetonitrile. After 2 h, the substrate was removed and rinsed with acetonitrile and ethanol, and dried with N_2. This process led to the formation of **S7-II**.

Cyclic voltammetry (CV) was carried out using an Autolab PGSTAT101 with NOVA Advanced Electrochemical Software. For the electrochemical experiments, a solution of 0.1 M of

https://doi.org/10.1021/acs.jpcc.2c02453
J. Phys. Chem. C 2022, 126, 13358−13365

Scheme 2. Synthesis of Urazole Precursor 6

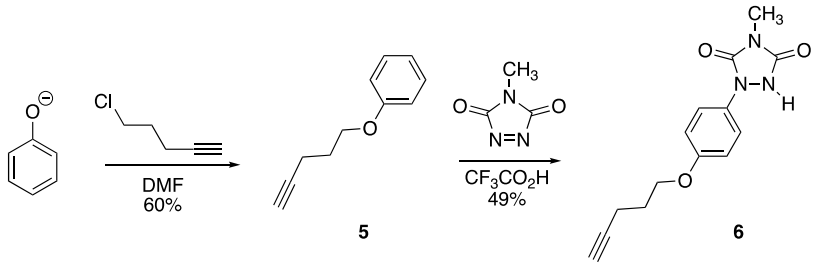

Scheme 3. Generation of Urazole Radical 7 and the Decomposition Pathway toward Dimer 8

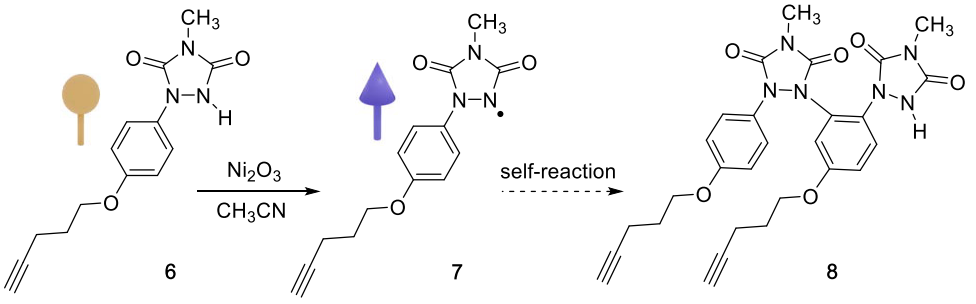

tetrabutylammonium hexafluorophosphate ($TBAPF_6$, 98%, Sigma) in dried acetonitrile was used as an electrolyte. The experiments were performed under inert conditions. For the characterization of the SAMs using a redox probe, we used a solution of 0.1 M KCl in Milli-Q water as electrolyte, containing 0.01 M of $[Fe(CN)_6]^{3-/4-}$ as redox marker. The bare Au or the functionalized surfaces were used as working electrodes. Finally, for characterizing the redox activity of **S7** SAMs, the functionalized substrates were used as a working electrode and Pt wires as counter and reference electrodes. The SAMs' coverage (Γ) was then calculated as follows[30]

$$\Gamma = \frac{Q}{n \cdot F \cdot A}$$

$$Q = \frac{A_{uc}}{SR}$$

where Q is the charge transferred, n is the number of electrons transferred, F is the Faraday constant, and A is the electrode area immersed in the solution. The charge transferred Q is obtained by the quotient of the area under the curve (A_{uc}) in the redox process through integration and the scan rate (SR).

Ultraviolet−visible (UV−vis) measurements were performed using a JASCO V-780 Spectrophotometer recorded at a 400 nm/s scan speed. Solutions with a concentration of 10^{-4} M of the urazole derivatives in acetonitrile were prepared.

Electron paramagnetic resonance spectroscopy (EPR) spectra were obtained using an X-Band (9.7 GHz) Bruker ELEXSYS E500 spectrometer equipped with a Bruker variable temperature unit, an ST8911 microwave cavity, a field frequency lock system Bruker ER 033 M, and a NMR Gaussmeter Bruker ER 035 M. The solutions containing 10^{-4} M urazole derivatives in acetonitrile were previously degassed with argon and measured in thin quartz tubes. SAM samples were measured in a Suprasil tissue cell.

Contact angle characterization was performed using a DSA100 System (KRÜSS) by automatically dispensing 3 μL of Milli-Q water drops. The measurements were carried out in triplicate.

X-ray photoelectron spectroscopy (XPS) measurements were performed at room temperature with a SPECS PHOIBOS 150 hemispherical analyzer (SPECS GmbH, Berlin, Germany) with a base pressure of 5×10^{-10} mbar using monochromatic Al Kα radiation (1486.74 eV) as an excitation source operated at 300 W. The energy resolution as measured by the full width at half maximum (FWHM) of the Ag $3d_{5/2}$ peak for a sputtered silver foil was 0.62 eV.

RESULTS AND DISCUSSION

Urazole radical precursor **6** (Scheme 2) was designed to include aryl-substitution similar to the previously investigated urazole **1b** but with the addition of a short alkoxy chain and a terminal alkyne group. The former provides some flexibility to the system, whereas the alkyne group has been previously shown to be a suitable Au surface anchor group that leads to a robust Au−C covalent bond.[31,32] Urazole **6** was synthesized according to Scheme 2. The reaction of 5-chloro-1-butyne with potassium phenoxide in dry DMF afforded aryl ether **5** in a 60% yield. The neat reaction of **5** with *N*-methyl-1,2,4-triazoline-3,5-dione (MeTAD) in the presence of trifluoroacetic acid as a catalyst, according to the procedure previously described for the reaction of MeTAD with anisole,[33] afforded the desired 1-substituted urazole **6** in a 49% yield (Figures S1−S4).

The formation of the radical derived from **6** was studied in solution following the previously reported methodology (Scheme 3).[26] Oxidation of **6** with the commercially available heterogeneous oxidant Ni_2O_3 in CH_3CN or $CDCl_3$ followed by filtration afforded a deep blue solution of radical **7**. The paramagnetic nature of the radical prevented direct observation of **7** by ^{1}H NMR spectroscopy, but over the course of several hours the signals for a new compound, dimer **8** began to appear (see Scheme 3). Complete consumption of **7** over several days, with a concomitant loss of the characteristic deep blue color, led primarily to the formation of **8**, which could be isolated in a 32% yield (Figures S5 and S6). Furthermore, attempts at isolating radical **7** via the concentration of

https://doi.org/10.1021/acs.jpcc.2c02453
J. Phys. Chem. C 2022, 126, 13358−13365

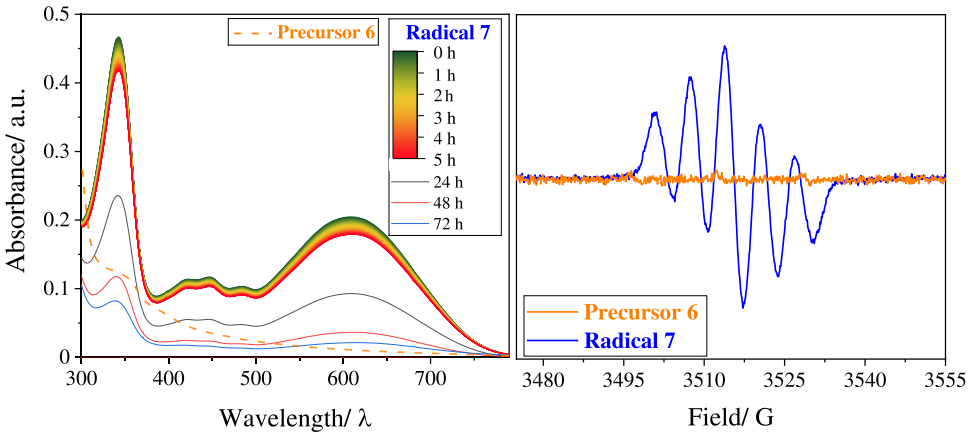

Figure 1. Left. UV−vis spectra of **6** and **7** in acetonitrile. The spectrum of **7** was registered over time ($c = 10^{-4}$ M). Right. EPR spectra of **6** and **7** in acetonitrile ($c = 10^{-4}$ M).

solutions promoted the formation of **8** (see Supporting Information).

The UV−vis spectrum of a freshly prepared solution of **7** in CH_3CN showed the characteristic absorption bands of this family of radicals (Figure 1, left).[25−27] Intense absorption bands at 343 and 609 nm are observed, accompanied by less intense bands centered at 420, 445, and 485 nm. The stability of the radical was assessed by following the UV−vis spectrum with time. The radical was found to be stable in solution for more than 5 h, observing only a small decrease in the absorption bands' intensity. However, in line with what had been observed via ^{1}H NMR spectroscopy, after 24 h, a significant drop in the absorption bands indicated the depletion of the radical due to the self-reaction of **7** to afford dimer **8** (Scheme 3).

The radical formation was also investigated by EPR spectroscopy in solution. As expected, precursor **6** was EPR silent due to its diamagnetic character (Figure 1, right). In contrast, radical **7** exhibited a five-line spectrum centered at g = 2.0034, close to the value of the free electron. The hyperfine splitting comes from the interaction of the radical with two equivalent ^{14}N nuclei, with coupling constant and bandwidth of a = 6.5 G and ΔH_{pp} = 3.1 G, respectively.[34]

CV characterization was performed employing a three-electrode electrochemical cell and using platinum wires as working and counter electrodes, and a Ag/AgCl reference electrode (Figure 2). In the case of radical **7**, a redox peak at $E^{1/2}$ = 227 mV, ascribed to the reduction of the radical to the anion form, was clearly observed (Scheme 4). At higher voltages, the CV exhibited an oxidation peak at $E^{1/2}$ = 1148 mV attributed to the oxidation of the radical to the diazonium species (Scheme 4).[26] In contrast, the CV of the radical precursor **6** only showed the oxidation peak to the diazonium form at $E^{1/2}$ = 1143 mV. These behaviors were consistent with what had been previously reported for urazole radical **2b**.[26]

Once we confirmed the successful formation of radical **7** and confirmed its stability over a time period of several hours in solution, we proceeded to the preparation of self-assembled monolayers of **7** on Au. With this aim, we followed two distinct routes (Figure 3). Approach I was focused on the formation of a SAM of urazole precursor **6** on the gold surface over 48 h. Following this, the SAM was then oxidized to generate radical **7** (**S7-I**) directly on the surface. Alternatively, in approach II, the radical was first separately generated in solution, and then the Au substrate was immersed in the radical solution for 2 h

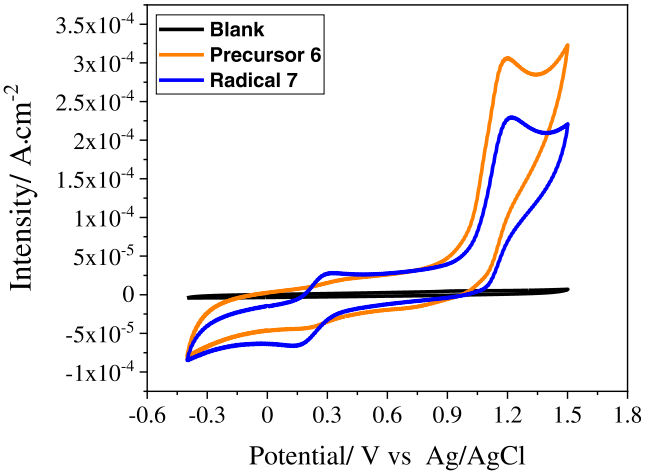

Figure 2. Cyclic voltammograms of **6** and **7** (10^{-4} M) in acetonitrile containing tetrabutylammonium hexafluorophosphate ($TBAPF_6$) 0.1 M. The Ag/AgCl electrode was used as reference and platinum wires as working and counter electrodes. Scan rate: 0.1 V s^{-1}. A blank acquired using a Pt wire is also included.

Scheme 4. Electrochemical Oxidation and Reduction Events of Urazole Radical 7 As Observed by Cyclic Voltammetry

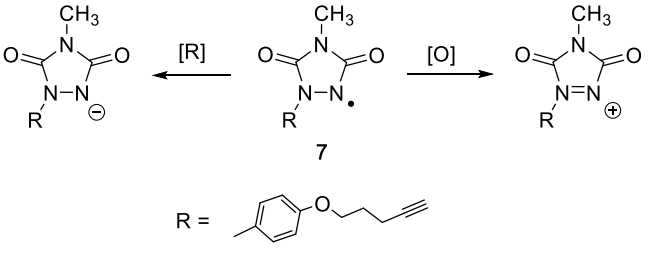

to form the corresponding radical SAM (**S7-II**). In both cases, the SAM formation processes were adjusted to find optimum conditions.

The SAMs from both approaches were fully characterized by X-ray photoelectron spectroscopy (XPS), water contact angle, EPR, and CV. C 1s and N 1s XPS data confirmed the presence of molecules **6** and **7** on the gold surface (Figure S7). By water contact angle, we observed a decrease in the angle from the bare gold substrate (84.8° ± 1.8°) to the functionalized substrates, giving a value of 52.4° ± 2.0° for **S6** and 49.7° ±

https://doi.org/10.1021/acs.jpcc.2c02453
J. Phys. Chem. C 2022, 126, 13358−13365

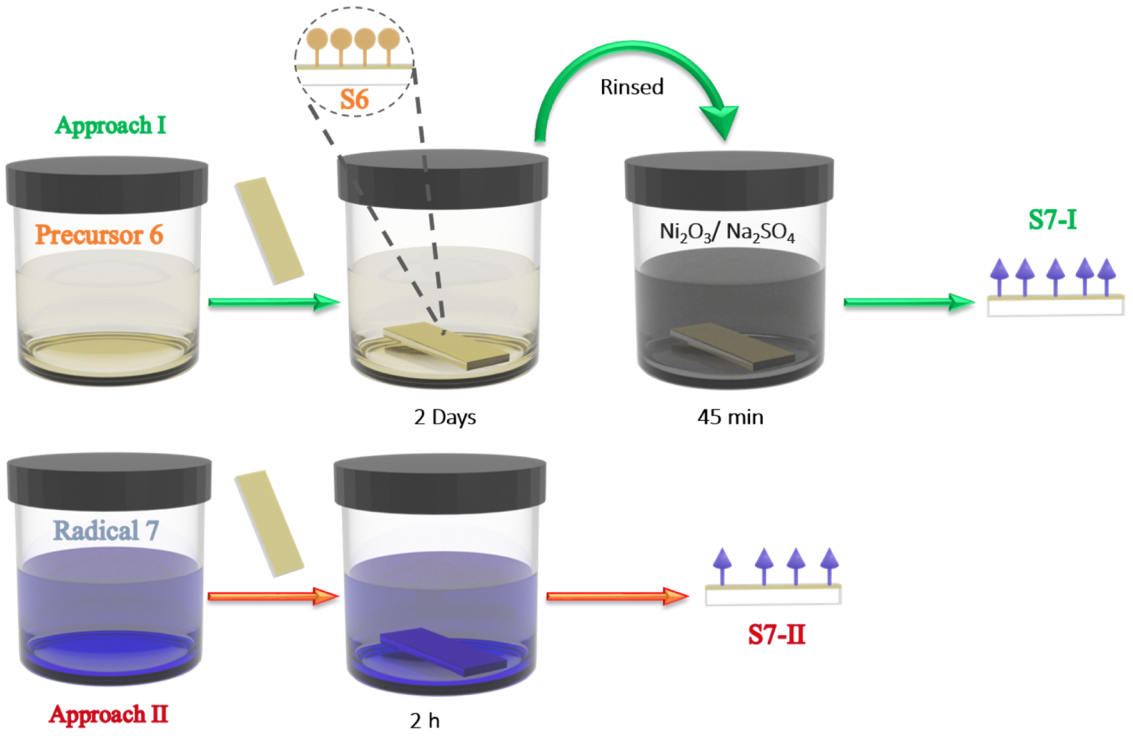

Figure 3. Schematic representation of the approaches used to prepare SAMs of radical **7**.

1.2° for **S7** (Figure S8). This behavior is consistent with the hydrophilic character of the surface-bound molecules.

EPR characterization was also carried out since it is a powerful tool for the identification of radicals on surfaces.[35] Figure 4 shows the spectra collected for the SAMs of **7**

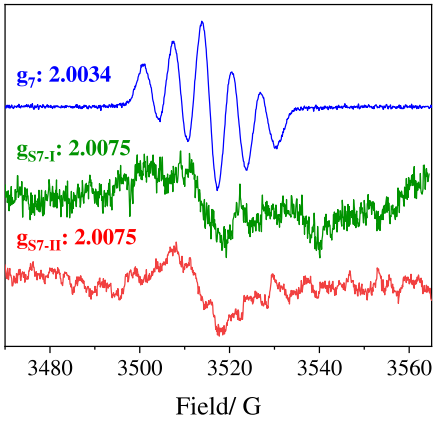

Figure 4. EPR spectra of **7** (blue) in solution and SAMs **S7-I** (green) and **S7-II** (red).

prepared according to the two approaches together with the EPR of the same molecule in solution. The SAMs show a weak but distinguishable line with a *g*-factor value (g = 2.0075) similar to that of the unbound radical in solution (g = 2.0034). Due to the low intensity of the signals and also their larger linewidth typical of solid-state measurements, the hyperfine couplings were not clearly observed. Nonetheless, this data proves unambiguously the presence of an unpaired spin on the functionalized gold surfaces.

CV was also used to verify the SAM formation. First, electrochemical experiments were carried out in a three-electrode configuration cell, using a Pt wire and an Ag/AgCl electrode as counter and reference electrodes, respectively. As working electrodes, a bare Au electrode and the functionalized substrates (**S7-I, II**) were employed. The electrolyte consisted of a 0.1 M KCl aqueous solution containing 10 mM $[Fe(CN)_6]^{3-/4-}$ as benchmark redox marker. As observed in Figure 5a, a decrease in the redox peak current intensity accompanied by a larger peak-to-peak separation (ΔE) is observed when the Au substrates covered with the SAMs are used instead of the bare Au electrode. This is rationalized by the passivation of the electrode with the surface-bound molecules that hinder the electron transfer process from the redox probe in solution to the electrode. It is noted that the $[Fe(CN)_6]^{3-/4-}$ redox peak is more inhibited with the **S7-I** substrate, which suggests that approach I leads to greater surface coverage.

CV experiments were also carried out with the aim of detecting the redox activity of the radical SAM. In this case, we registered the electrochemical response of the **S7** SAMs. We used a 10^{-4} M $TBAPF_6$ solution in acetonitrile as an electrolyte, a Pt wire as a pseudo-reference electrode, and **S7-I, II** as working electrodes. For both approaches, a reversible redox peak attributed to the reduction of the radical to the anion (see Scheme 4) was detected at $E^{1/2}$ = 21 mV and $E^{1/2}$ = −40 mV, for **S7-I, II**, respectively (Figure 5b). Notice that the oxidation redox process to the diazonium species (see Scheme 4) could not be investigated since the SAMs are not stable under the application of very high voltage values.[36] The intensity of the redox peaks linearly increased with the scan rate (Figure S9), which is characteristic of surface-confined species.[23] The differences in shape and redox potential values between the two substrates may be attributed to the distinct molecular organizations resulting from the two different methods of SAM preparation.[37] It has been reported that changes in the local intermolecular and electrostatic interactions induced by the supramolecular organization and

https://doi.org/10.1021/acs.jpcc.2c02453
J. Phys. Chem. C 2022, 126, 13358−13365

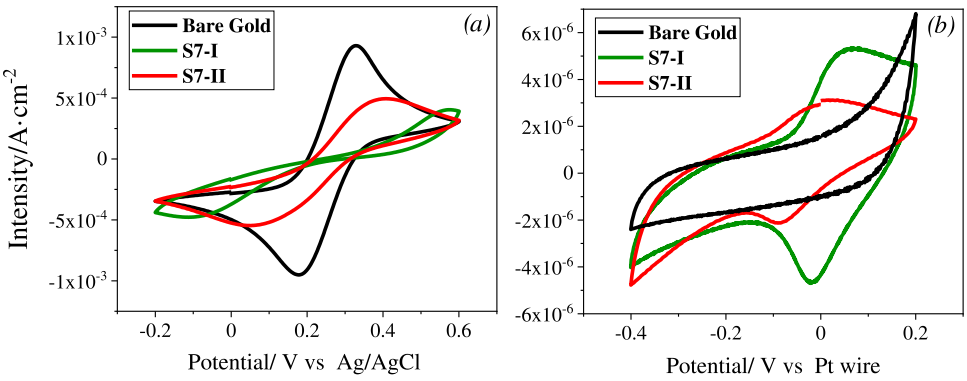

Figure 5. Electrochemical characterization of **S7-I** (green) and **S7-II** (red). (a) Redox probe experiment carried out using a solution of 0.1 M KCl as an electrolyte in Milli-Q water with 0.01 M $[Fe(CN)_6]^{3-/4-}$ as a redox marker. The bare Au or the functionalized surfaces were used as working electrodes, a Pt wire as a counter electrode, and a Ag/AgCl electrode as a reference. (b) CV measurements performed by immersion of the modified electrodes in acetonitrile containing 10^{-4} M $TBAPF_6$ and using Pt wires as counter and pseudo-reference. Scan rate: 0.1 V s^{-1}.

distribution of the redox active species within the layer may lead to different electrochemical voltammograms (e.g., peak shifting, peak splitting, or peak broadening).[37−39] By integration of the redox peaks (see the Experimental Section), surface coverages of 5.0×10^{-10} and 1.2×10^{-11} mol cm^{-2} were estimated for **S7-I** and **S7-II**, respectively. The greater surface coverage measured for **S7-I** agrees with the results using the redox marker as discussed earlier. While the lower surface coverage of **S7-II** might at first glance be rationalized by the shorter time period allowed for SAM formation in approach II than that provided in approach I, it was observed that longer incubation times did not increase the radical density on the surface, as determined by CV. Likely, the self-reaction of radical **7** in solution during SAM formation (see Scheme 2) resulted in competing grafting of dimer **8** onto the surface. Such dimerized molecules would not be electroactive in this region and, hence, are not considered in the estimation of the surface coverage.

Finally, density functional theory calculations were performed to understand the configuration of the molecules adsorbed on the surface (see Supporting Information for computational details). It was found that the molecules tend to be vertical with respect to the surface and, as a first approximation, the maximum molecular density calculated (approx. 7×10^{-10} mol cm^{-2}) was found to be slightly higher than the value estimated in approach I by CV (Figure S10).

CONCLUSIONS

In summary, we have demonstrated that SAMs of 1-arylurazole radicals can be successfully prepared by two different approaches despite their limited lifetimes in solution and inability to isolate them in the solid state. The SAM with greater urazole radical surface coverage and, thus, electrochemical activity was achieved by first grafting the urazole precursor to the gold surface prior to oxidation of the precursor to the active radical species. In both instances, however, analysis by both EPR and CV clearly demonstrates radical behavior similar to that exhibited by the urazole radical in solution. In this investigation, therefore, we have successfully developed and optimized the conditions for future studies of other urazole radical SAMs. Of particular interest would be the investigation of urazole radicals known to be longer-lived in solution.[25]

ASSOCIATED CONTENT

Supporting Information

The Supporting Information is available free of charge at https://pubs.acs.org/doi/10.1021/acs.jpcc.2c02453.

^{1}H and ^{13}C NMR spectra of **5**, **6**, and **8**, XPS and contact angle of **S6** and **S7**, and CV measurements at different scan rates of **S7-I, II** (PDF)

AUTHOR INFORMATION

Corresponding Authors

Núria Crivillers − *Institut de Ciència de Materials de Barcelona, ICMAB-CSIC, 08193 Bellaterra, Spain;* orcid.org/0000-0001-6538-2482; Email: ncrivillers@icmab.es

Gary W. Breton − *Department of Chemistry and Biochemistry, Berry College, Mount Berry, Georgia 30149, United States;* orcid.org/0000-0001-5760-7071; Email: gbreton@berry.edu

Marta Mas-Torrent − *Institut de Ciència de Materials de Barcelona, ICMAB-CSIC, 08193 Bellaterra, Spain;* orcid.org/0000-0002-1586-005X; Email: mmas@icmab.es

Authors

Ángel Campos-Lendinez − *Institut de Ciència de Materials de Barcelona, ICMAB-CSIC, 08193 Bellaterra, Spain*

Stefan T. Bromley − *Departament de Ciència de Materials i Física Química & Institut de Química Teòrica i Computacional (IQTCUB), Universitat de Barcelona, E-08028 Barcelona, Spain; Institució Catalana de Recerca i Estudis Avançats (ICREA), E-08010 Barcelona, Spain;* orcid.org/0000-0002-7037-0475

Concepció Rovira − *Institut de Ciència de Materials de Barcelona, ICMAB-CSIC, 08193 Bellaterra, Spain;* orcid.org/0000-0002-2365-9479

Complete contact information is available at: https://pubs.acs.org/10.1021/acs.jpcc.2c02453

Notes

The authors declare no competing financial interest.

ACKNOWLEDGMENTS

This work was funded by the Spanish Ministry with the project GENESIS PID2019-111682RB-I00 and through the "Severo

Ochoa" Programme for Centers of Excellence in R&D (FUNFUTURE CEX2019-000917-S) and the Generalitat de Catalunya (2017-SGR-918). Á.C.-L. is enrolled in the UAB Materials Science PhD program. G.B. thanks Berry College for generous financial support. S.T.B. acknowledges financial support from the Spanish Ministerio de Ciencia, Innnovación y Universidades (RTI2018-095460-B-100, and MDM-2017-0767 via the Spanish Structures of Excellence María de Maeztu program), the Generalitat de Catalunya (2017SGR13), and the Red Espanola de Supercomputación (RES) for the provision of supercomputing time.

REFERENCES

(1) De Ruiter, G.; Gupta, T.; Van Der Boom, M. E. Selective Optical Recognition and Quantification of Parts per Million Levels of Cr6+ in Aqueous and Organic Media by Immobilized Polypyridyl Complexes on Glass. *J. Am. Chem. Soc.* **2008**, *130*, 2744−2745.

(2) Basabe-Desmonts, L.; Beld, J.; Zimmerman, R. S.; Hernando, J.; Mela, P.; García Parajó, M. F.; Van Hulst, N. F.; Van Den Berg, A.; Reinhoudt, D. N.; Crego-Calama, M. A Simple Approach to Sensor Discovery and Fabrication on Self-Assembled Monolayers on Glass. *J. Am. Chem. Soc.* **2004**, *126*, 7293−7299.

(3) Muñoz, J.; Campos-Lendinez, Á.; Crivillers, N.; Mas-Torrent, M. Selective Discrimination of Toxic Polycyclic Aromatic Hydrocarbons in Water by Targeting π-Stacking Interactions. *ACS Appl. Mater. Interfaces* **2020**, *12*, 26688−26693.

(4) Ricci, S.; Casalini, S.; Parkula, V.; Selvaraj, M.; Saygin, G. D.; Greco, P.; Biscarini, F.; Mas-Torrent, M. Label-Free Immunodetection of α-Synuclein by Using a Microfluidics Coplanar Electrolyte-Gated Organic Field-Effect Transistor. *Biosens. Bioelectron.* **2020**, *167*, No. 112433.

(5) Mendes, P. M. Stimuli-Responsive Surfaces for Bio-Applications. *Chem. Soc. Rev.* **2008**, *37*, 2512−2529.

(6) Artzy-Schnirman, A.; Brod, E.; Epel, M.; Dines, M.; Hammer, T.; Benhar, I.; Reiter, Y.; Sivan, U. A Two-State Electronic Antigen and an Antibody Selected to Discriminate between These States. *Nano Lett.* **2008**, *8*, 3398−3403.

(7) Simão, C.; Mas-Torrent, M.; Veciana, J.; Rovira, C. Multichannel Molecular Switch with a Surface-Confined Electroactive Radical Exhibiting Tunable Wetting Properties. *Nano Lett.* **2011**, *11*, 4382−4385.

(8) Colorado, R.; Lee, T. R. Wettabilities of Self-Assembled Monolayers on Gold Generated from Progressively Fluorinated Alkanethiols. *Langmuir* **2003**, *19*, 3288−3296.

(9) Heimel, G.; Romaner, L.; Zojer, E.; Bredas, J. L. The Interface Energetics of Self-Assembled Monolayers on Metals. *Acc. Chem. Res.* **2008**, *41*, 721−729.

(10) Herrmann, C.; Solomon, G. C.; Ratner, M. A. Organic Radicals As Spin Filters. *J. Am. Chem. Soc.* **2010**, *132*, 3682−3684.

(11) Mas-Torrent, M.; Crivillers, N.; Rovira, C.; Veciana, J. Attaching Persistent Organic Free Radicals to Surfaces: How and Why. *Chem. Rev.* **2012**, *112*, 2506−2527.

(12) Ratera, I.; Vidal-Gancedo, J.; Maspoch, D.; Bromley, S. T.; Crivillers, N.; Mas-Torrent, M. Perspectives for Polychlorinated Trityl Radicals. *J. Mater. Chem. C* **2021**, *9*, 10610−10623.

(13) Zhang, Y. H.; Kahle, S.; Herden, T.; Stroh, C.; Mayor, M.; Schlickum, U.; Ternes, M.; Wahl, P.; Kern, K. Temperature and Magnetic Field Dependence of a Kondo System in the Weak Coupling Regime. *Nat. Commun.* **2013**, *4*, No. 2110.

(14) Liu, J.; Isshiki, H.; Katoh, K.; Morita, T.; Breedlove, B. K.; Yamashita, M.; Komeda, T. First Observation of a Kondo Resonance for a Stable Neutral Pure Organic Radical, 1,3,5-Triphenyl-6-Oxoverdazyl, Adsorbed on the Au(111) Surface. *J. Am. Chem. Soc.* **2013**, *135*, 651−658.

(15) Müllegger, S.; Rashidi, M.; Fattinger, M.; Koch, R. Surface-Supported Hydrocarbon π Radicals Show Kondo Behavior. *J. Phys. Chem. C* **2013**, *117*, 5718−5721.

(16) Mas-Torrent, M.; Crivillers, N.; Mugnaini, V.; Ratera, I.; Rovira, C.; Veciana, J. Organic Radicals on Surfaces: Towards Molecular Spintronics. *J. Mater. Chem.* **2009**, *19*, 1691−1695.

(17) Poggini, L.; Cucinotta, G.; Pradipto, A. M.; Scarrozza, M.; Barone, P.; Caneschi, A.; Graziosi, P.; Calbucci, M.; Cecchini, R.; Dediu, V. A.; et al. An Organic Spin Valve Embedding a Self-Assembled Monolayer of Organic Radicals. *Adv. Mater. Interfaces* **2016**, *3*, No. 1500855.

(18) Simão, C.; Mas-Torrent, M.; Crivillers, N.; Lloveras, V.; Artés, J. M.; Gorostiza, P.; Veciana, J.; Rovira, C. A Robust Molecular Platform for Non-Volatile Memory Devices with Optical and Magnetic Responses. *Nat. Chem.* **2011**, *3*, 359−364.

(19) Finklea, H. O.; Madhiri, N. Reorganization Energies of TEMPO{radical Dot}/TEMPO+ in Water. *J. Electroanal. Chem.* **2008**, *621*, 129−133.

(20) Alévêque, O.; Seladji, F.; Gautier, C.; Dias, M.; Breton, T.; Levillain, E. Nitroxyl Radical Self-Assembled Monolayers on Gold: Versatile Electroactive Centers in Aqueous and Organic Media. *ChemPhysChem* **2009**, *10*, 2401−2404.

(21) Matsushita, M. M.; Ozaki, N.; Sugawara, T.; Nakamura, F.; Hara, M. Formation of Self-Assembled Monolayer of Phenylthiol Carrying Nitronyl Nitroxide on Gold Surface. *Chem. Lett.* **2002**, *31*, 596−597.

(22) Mannini, M.; Sorace, L.; Gorini, L.; Piras, F. M.; Caneschi, A.; Magnani, A.; Menichetti, S.; Gatteschi, D. Self-Assembled Organic Radicals on Au(111) Surfaces: A Combined ToF-SIMS, STM, and ESR Study. *Langmuir* **2007**, *23*, 2389−2397.

(23) Crivillers, N.; Mas-Torrent, M.; Vidal-Gancedo, J.; Veciana, J.; Rovira, C. Self-Assembled Monolayers of Electroactive Polychlorotriphenylmethyl Radicals on Au(111). *J. Am. Chem. Soc.* **2008**, *130*, 5499−5506.

(24) Ajayakumar, M. R.; Moreno, C.; Alcón, I.; Illas, F.; Rovira, C.; Veciana, J.; Bromley, S. T.; Mugarza, A.; Mas-Torrent, M. Neutral Organic Radical Formation by Chemisorption on Metal Surfaces. *J. Phys. Chem. Lett.* **2020**, *11*, 3897−3904.

(25) Pirkle, W. H.; Gravel, P. L. Persistent Cyclic Diacylhydrazyl Radicals from Urazoles and Pyrazolidine-3,5-Diones. *J. Org. Chem.* **1978**, *43*, 808−815.

(26) Breton, G. W.; Suroviec, A. H. Intermediacy of a Persistent Urazole Radical and an Electrophilic Diazenium Species in the Acid-Catalyzed Reaction of MeTAD with Anisole. *J. Org. Chem.* **2016**, *81*, 206−214.

(27) Breton, G. W. Factors Affecting the Dimerization of Persistent Nitrogen - Centered 1 - Phenyl Urazole Radicals to Tetrazanes. *J. Phys. Org. Chem.* **2018**, *31*, No. e3808.

(28) Billiet, S.; De Bruycker, K.; Driessen, F.; Goossens, H.; Van Speybroeck, V.; Winne, J. M.; Du Prez, F. E. Triazolinediones Enable Ultrafast and Reversible Click Chemistry for the Design of Dynamic Polymer Systems. *Nat. Chem.* **2014**, *6*, 815−821.

(29) Breton, G. W.; Turlington, M. Alternative Synthetic Routes to N-Methyl-1,2,4-Triazoline-3,5-Dione (MeTAD) and Other Triazolinedione Derivatives. *Tetrahedron Lett.* **2014**, *55*, 4661−4663.

(30) Haag, A. L.; Toader, V.; Lennox, R. B.; Grutter, P. Selective in Situ Potential-Assisted SAM Formation on Multi Electrode Arrays. *Nanotechnology* **2016**, *27*, No. 455501.

(31) Li, Q.; Han, C.; Fuentes-Cabrera, M.; Terrones, H.; Sumpter, B. G.; Lu, W.; Bernholc, J.; Yi, J.; Gai, Z.; Baddorf, A. P.; et al. Electronic Control over Attachment and Self-Assembly of Alkyne Groups on Gold. *ACS Nano* **2012**, *6*, 9267−9275.

(32) De Sousa, J. A.; Bejarano, F.; Gutiérrez, D.; Leroux, Y. R.; Nowik-Boltyk, E. M.; Junghoefer, T.; Giangrisostomi, E.; Ovsyannikov, R.; Casu, M. B.; Veciana, J.; et al. Exploiting the Versatile Alkyne-Based Chemistry for Expanding the Applications of a Stable Triphenylmethyl Organic Radical on Surfaces. *Chem. Sci.* **2020**, *11*, 516−524.

(33) Breton, G. W. Acid-Catalyzed Reaction of 4-Methyl-1,2,4-Triazoline-3,5-Dione (MeTAD) with Substituted Benzenes. *Tetrahedron Lett.* **2011**, *52*, 733−735.

https://doi.org/10.1021/acs.jpcc.2c02453
J. Phys. Chem. C 2022, 126, 13358−13365

(34) Sahu, I. D.; Lorigan, G. A.; States, U. *EPR Techniques, Spin Labeling, and Spin Trapping*, 3rd ed.; Elsevier Ltd.: Amsterdam, The Netherlands, 2019.
(35) Crivillers, N.; Mas-Torrent, M.; Perruchas, S.; Roques, N.; Vidal-Gancedo, J.; Veciana, J.; Rovira, C.; Basabe-Desmonts, L.; Ravoo, B. J.; Crego-Calama, M.; Reinhoudt, D. N. Self-Assembled Monolayers of a Multifunctional Organic Radical. *Angew. Chem.* **2007**, *119*, 2265−2269.
(36) Casado-Montenegro, J.; Marchante, E.; Crivillers, N.; Rovira, C.; Mas-Torrent, M. Donor/Acceptor Mixed Self-Assembled Monolayers for Realising a Multi-Redox-State Surface. *ChemPhysChem* **2016**, *17*, 1810−1814.
(37) Alévêque, O.; Blanchard, P. Y.; Breton, T.; Dias, M.; Gautier, C.; Levillain, E.; Seladji, F. Nitroxyl Radical Self-Assembled Monolayers on Gold: Experimental Data vs. Laviron's Interaction Model. *Electrochem. Commun.* **2009**, *11*, 1776−1780.
(38) Duffin, T. J.; Nerngchamnong, N.; Thompson, D.; Nijhuis, C. A. Direct Measurement of the Local Field within Alkyl-Ferrocenyl-Alkanethiolate Monolayers: Importance of the Supramolecular and Electronic Structure on the Voltammetric Response and Potential Profile. *Electrochim. Acta* **2019**, *311*, 92−102.
(39) Guo, Y.; Zhao, J.; Zhu, J. Study on the Intermolecular Interactions between the Functional Moieties in Ferrocene-Terminated Alkanethiol Self-Assembled Monolayer on Gold. *Thin Solid Films* **2008**, *516*, 3051−3057.

https://doi.org/10.1021/acs.jpcc.2c02453
J. Phys. Chem. C 2022, 126, 13358−13365